fluids

MDPI

Article

Non-Newtonian Convective Heat Transfer in Annuli: Numerical Investigation on the Effects of Staggered Helical Fins

Luca Pagliarini [1,*], Fabio Bozzoli [2,3], Rasoul Fallahzadeh [1] and Sara Rainieri [1,3]

[1] Department of Engineering and Architecture, University of Parma, Parco Area delle Scienze 181/A, 43124 Parma, Italy; rasoul.fallahzadeh@unipr.it (R.F.); sara.rainieri@unipr.it (S.R.)
[2] Department of Engineering for Industrial Systems and Technologies—DISTI, University of Parma, Parco Area delle Scienze 181/A, 43124 Parma, Italy; fabio.bozzoli@unipr.it
[3] SITEIA.PARMA Interdepartmental Centre, University of Parma, Parco Area delle Scienze 181/A, 43124 Parma, Italy
* Correspondence: luca.pagliarini@unipr.it

Abstract: Despite non-Newtonian fluids being involved in many industrial processes, e.g., in food and chemical industries, their thermal treatment still represents a significant challenge due to their generally high apparent viscosity and consequent low heat transfer capability. Heat transfer in heat exchangers can be enhanced by passive systems, such as inserts or fins, to promote boundary layer disruption and fluid recirculation. However, most of the existing configurations cannot significantly improve the heat transfer over pressure drops in deep laminar flows. The present paper presents a numerical investigation on non-Newtonian flows passing through the annulus side of a double-pipe heat exchanger with staggered helical fins. The adopted geometry was conceptualized by merging the beneficial effects of swirling flow devices and boundary layer disruption. The numerical results were first validated against analytical solutions for non-Newtonian flows in annuli under a laminar flow regime. The finned geometry was therefore numerically tested and compared with the bare annulus to quantify the resulting heat transfer augmentation. When compared with the bare annuli, the proposed novel geometry greatly enhanced the heat transfer while mitigating friction losses.

Keywords: double-pipe heat exchangers; non-Newtonian flows; annular sections; passive heat transfer augmentation; computational fluid dynamics

Citation: Pagliarini, L.; Bozzoli, F.; Fallahzadeh, R.; Rainieri, S. Non-Newtonian Convective Heat Transfer in Annuli: Numerical Investigation on the Effects of Staggered Helical Fins. *Fluids* **2024**, *9*, 272. https://doi.org/10.3390/fluids9120272

Academic Editors: Leonardo Di G. Sigalotti, Carlos Enrique Alvarado-Rodríguez and Wei-Tao Wu

Received: 5 November 2024
Revised: 18 November 2024
Accepted: 20 November 2024
Published: 21 November 2024

1. Introduction

Heat transfer augmentation in heat exchangers (HEs) has been extensively pursued in past decades due to stricter and stricter economic and environmental standards required by the general industry [1]. Thanks to its compactness, modular construction, simple maintenance and cost-effectiveness, the double-pipe heat exchanger (DPHE) represents one of the most employed layouts for industrial applications, including thermal energy storage, waste heat recovery, power generation and fluids treatment [2]. Higher DPHE efficiencies can be achieved by adopting either active or passive methods, or combinations of both [3]. Active solutions require external forces to perturb the fluid flow, i.e., through magnetic fields or rotating elements. On the other hand, passive methods do not require any auxiliary equipment, and they are thus generally preferable. In fact, to ensure high fluid recirculation and boundary layer disruption, passive solutions may rely either on modified geometries (e.g., tube corrugations or helical layouts) or on tube inserts (e.g., fins or coiled wires in the annulus side or in the inner tube) [4].

The beneficial effect of passive solutions on thermal performance is further increased when highly viscous flows, such as non-Newtonian fluids, are processed, as in chemical and food industries. Here, heat transfer enhancement becomes crucial to obtain higher fluid thermalization, which helps preserve the product characteristics during processing [5], as well as extending the shelf life.

Despite most of the literature works proposing heat transfer enhancement solutions for Newtonian flows [3,4], few scholars focused on the effects of passive techniques on non-Newtonian flows in DPHEs. Ghanbari and Javaherdeh [6] experimentally analyzed graphene nanofluid flow through an annular section with perforated baffles in a turbulent regime. Baffles with 16 holes ensured the greatest thermal performance factor (equal to 1.29), and they improved the heat transfer at all Reynolds numbers. Yaghoubzadeh and Javaherdeh [7] numerically designed porous rings in the annulus side of a DPHE to achieve heat transfer enhancement for a nanofluid turbulent flow. Different geometrical parameters, such as the number, height and thickness of the porous rings, were studied and compared. The employment of six porous rings 2 mm high and 6 mm thick guaranteed, for a Reynolds number equal to 4000, a maximum improved efficiency of 11.25%. A similar porous rings solution was therefore investigated experimentally in terms of the heat transfer, pressure dops and heat transfer performance ratio [8]. Further investigations on non-Newtonian fluids through the annulus side of DPHEs were performed by considering the extended surfaces of different shapes [9–14].

However, although the mentioned turbulators introduce high flow perturbances that lead to enhanced thermal performances, their application is not recommended for those applications in which fouling represents a major issue (as in food processing [15]) due to the frequent occurrence of fluid stagnation. Hence, some works focused on swirling flow devices capable of improving the overall performance of DPHEs without abruptly perturbing the fluid flow. Mozafarie and Javaherdeh [16] numerically studied the effects of helical fins in the annulus side of a DPHE under a laminar regime. Soursop juice at 24.3 °Brix was used as the process fluid. Different helical pitches (from 25 to 100 mm) and mass flow rates (from 0.3 to 0.7 kg/s) were considered. In general, the best thermofluidic performance was achieved at a high pitch (100 mm), while poorer performances were obtained for lower pitches due to higher pressure drops. Karimi et al. [17] performed numerical simulations of a DPHE that had an inner tube equipped with a tape insert. The effects of different pitch ratios on the laminar and turbulent flows were investigated at varying volume fractions of the adopted nanofluid. The authors reported a higher Nusselt number and lower friction factor for higher nanofluid concentrations, as well as better thermofluidic performances through higher pitch inserts at higher Reynolds numbers, in accordance with [16]. The reason behind the lower efficiency at lower Reynolds numbers here was attributed to a weaker rotational flow, which was not able to significantly increase the heat exchange over the pressure drops. Such a remark disagrees with the general literature on swirling flow inserts, which are generally preferrable for laminar rather than turbulent regimes [4,18]. However, it must be stressed that according to [19,20], swirling flow systems in annular passages cannot effectively promote swirling motion when the Reynolds number is lower than $21/\delta$, where δ is the twist ratio of the helical inserts. In this case, referred to as a deep laminar regime, the effectiveness of passive heat transfer augmentation solutions may be undermined, representing a huge drawback for many practical applications.

Some researchers proposed further heat transfer enhancement solutions based on interruptions of the inserts or on staggered geometries. The overall beneficial effect introduced by such geometrical modifications resides in a greater fluid flow disturbance similar to that achieved by turbulators, which results in less frequent stagnation of the processed fluid. Mohosen et al. [21] experimentally investigated different fin configurations in the annulus side of a DPHE, including interrupted longitudinal rectangular fins. Cold and hot water were circulated at different Reynolds numbers in the outer and inner tubes, respectively. For all the test conditions, the interrupted fins presented an increased heat transfer coefficient and friction factor with respect to the circular and helical ones. Maakoul et al. [22] disclosed additional thermofluidic features of the longitudinal fins interruption through numerical simulations, with the aim of improving the global performance of a DPHE involving the cooling of liquids with a large Prandtl number and low Reynolds number (lower than about 350). A total of 24 fins were considered, with 333.33 mm and 166.66 mm split intervals and a fin rotation of 7.5° between two consecutive intervals. Specifically, peaks in the local heat transfer coefficient were located at the split points, confirming effective boundary layers disruption, especially for smaller split intervals. The authors reported that for the same pumping power, the heat transfer enhancement achieved was greater than that of continuous longitudinal fins by a maximum of 48%. Wang et al. [23] designed and numerically tested a novel geometry of continuous helical fins with a staggered layout. The effect of the torsion angle and the number of staggered sections was investigated through the theory of field synergy. Despite the considered regime being turbulent, the proposed configuration was capable of significantly reducing the drag over the heat transfer augmentation for a high number of staggered sections and a high torsion angle.

Furthermore, among the passive heat transfer augmentation methods for DPHEs, swirling flow devices (e.g., helical fins) provide good thermal performances and low fouling/fluid stagnation. For deep laminar regimes, their efficacies can nonetheless be undermined by a poorly induced swirling flow; interruptions in the geometrical configuration may represent an effective solution to enhancing the boundary layer disruption in non-Newtonian flows.

Hence, the aim of the present work was to numerically design and investigate a novel geometry constituted by an interrupted configuration of staggered helical fins in the annulus side of a DPHE to achieve heat transfer augmentation in deep laminar flows. In other words, the proposed arrangement was based on the concepts of both turbulator inserts and swirling flow devices in terms of the overall effects on the fluid flow and heat transfer. In fact, the present layout was expected to simultaneously ensure flow perturbation and rotational fluid motion by staggered and interrupted helical fins while mitigating the occurrence of fluid stagnation. To the authors' best knowledge, this represents one of the first attempts to numerically investigate interrupted staggered fin solutions in DPHEs for non-Newtonian fluids processing. It has to be underlined that results on the finned module were computed here through numerical rather than analytical means due to the intrinsic unfeasibility of finding analytical solutions to the three-dimensional thermo-fluid dynamics that occurred in the studied configuration. The numerical approach was first validated through analytical results for the bare annulus. The novel configuration was therefore numerically tested at different generalized Reynolds numbers and different rheological properties of the process fluid. Thermofluidic features of the fluid flow are discussed through dimensionless velocities and temperature contours. The friction factor and the Nusselt number were finally estimated to assess the effectiveness of the novel geometry.

2. Materials and Methods

The procedure employed in the present study was based on the following steps. First, the analytical solution for the annular section with a radius ratio $\omega = R_i/R_o = 0.57$ (R_i: inner radius, R_o: outer radius) and heated with a uniform heat flux boundary condition at the inner wall surface (adiabatic outer wall) was implemented for the non-Newtonian case. The solution referred to the bare annulus used as the benchmark solution to validate the numerical approach consequently adopted for the finned section. The value of the radius ratio was selected due to its relevance in industrial applications, especially in the food industry. The analytical results were therefore compared with the numerical results to assess the robustness of the numerical approach. Once the numerical scheme was successfully validated, the finned geometry with stainless steel fins was numerically tested for different generalized Reynolds numbers Re_g (in the range $1.5 < Re_g < 11$) and varying rheological properties.

2.1. Finned Geometry

The analyzed finned module was intended to be employed in the annulus side of a DPHE as a passive heat transfer augmentation solution. Its geometry, constituted by six stationary fins twisted around the inner surface of the annular passage, is depicted in Figure 1, where L is the length of the considered module.

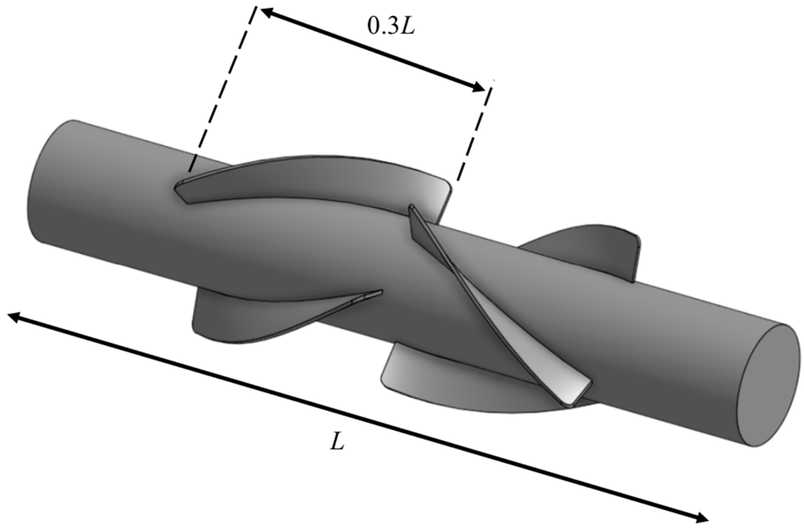

Figure 1. Finned geometry and geometrical references.

The fins are interrupted in the middle of the section of interest, and they proceed in a staggered configuration (i.e., opposite twisting angle) after 0.014*L*.

2.2. Mathematical Formulation

For the considered non-Newtonian power-law fluid flow through the annular pipe of Figure 2, the following assumptions and conditions were used:

- Incompressible, fully developed, steady-state, laminar and axis-symmetric forced flow;
- Negligible viscous dissipations;
- Constant thermal properties;
- Negligible axial conduction.

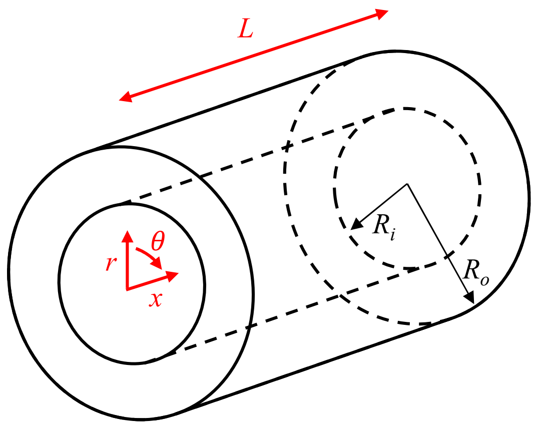

Figure 2. Annular pipe and reference system.

The continuity, momentum and energy equations for the present thermo-fluid dynamics problem read as follows [24]:

$$\nabla \cdot \boldsymbol{u} = 0 \tag{1a}$$

$$\rho \boldsymbol{u} \cdot \nabla \boldsymbol{u} = -\nabla p + \nabla \cdot \boldsymbol{\tau} \tag{1b}$$

$$\boldsymbol{u} \cdot \nabla T = \alpha \nabla^2 T \tag{1c}$$

where $\boldsymbol{u}$ is the velocity vector, p is the fluid pressure, $\boldsymbol{\tau}$ is the stress tensor, T is the temperature, ρ is the density and α is the thermal diffusivity. Note that Equations (1a)–(1c) appear in their general formulation for purely viscous fluids, and they can hence describe the thermo-fluid dynamics of either Newtonian or non-Newtonian fluids, depending on the employed definition of the stress tensor [25]. To characterize the rheology of the adopted non-Newtonian fluids, a power-law model correlating the local shear stress τ_{rx} to the local shear rate $\frac{\partial u}{\partial r}$ as $\tau_{rx} = m\left(\frac{\partial u}{\partial r}\right)^n$ was adopted, where m is the consistency index and n is the flow behavior index. The apparent viscosity of non-Newtonian power-law fluids can be thus formulated as a function of m and n: $\eta = m\left(\frac{\partial u}{\partial r}\right)^{n-1}$. For the present investigation, the rheological properties of typical highly viscous food products (e.g., tomato pastes) were considered with reference to the temperature ranges during a warming-up process [26]; under this approach, the chosen values for the consistency and the flow behavior indexes were as follows:

- ***Fluid 1*:** m = 22.43 Pa s^n, n = 0.46;
- ***Fluid 2*:** m = 76.15 Pa s^n, n = 0.28.

Such values are, in fact, interesting for the food industry, where the performance augmentation of DPHEs plays a crucial role (e.g., in pasteurization [27]). Equations of momentum and energy are completed by the following boundary and periodic conditions:

$$\boldsymbol{u}(r,x) = \boldsymbol{u}(r,x+L) \tag{2a}$$

$$k\left.\frac{\partial T(r,x)}{\partial r}\right|_{r=R_i} = q_w \tag{2b}$$

$$\left.\frac{\partial T(r,x)}{\partial r}\right|_{r=R_o} = 0 \tag{2c}$$

$$\frac{q_w A}{Q_m c_p} = T_b(x+L) - T_b(x) \tag{2d}$$

where L is the distance between the inlet and outlet of the periodic domain, k is the thermal conductivity, q_w is the heat flux, A the heat transfer area, Q_m is the mass flow rate, c_p is the specific heat and T_b is the bulk temperature.

2.3. Analytical Approach

For what concerns the fluid dynamics problem, Hanks and Larsen [28] proposed an analytical expression linking the volumetric flow rate Q_v with the pressure drop ΔP in non-Newtonian power-law fluids under a laminar flow:

$$Q_v = \frac{\pi n D_o^3}{8(3n+1)}\left(\frac{D_o \Delta p}{4\text{mL}}\right)^s \left[\left(1-\lambda^2\right)^{\frac{n+1}{n}} - \omega^{\frac{n-1}{n}}\left(\lambda^2-\omega^2\right)^{\frac{n+1}{n}}\right] \tag{3}$$

where $s = \frac{1}{n}$, and $\lambda(n,\omega)$ is the radial location of maximum velocity, formally obtained through the condition $u_1(\lambda) = u_2(\lambda)$, where u_1 and u_2 are the two terms of the radial velocity distribution:

$$\begin{cases} u_1 = R_o\left(\frac{\Delta P R_o}{2\text{mL}}\right)^s \int_\omega^\xi \left(\frac{\lambda^2}{r} - r\right)^s dr \quad if\ \omega \le \xi \le \lambda \\ u_2 = R_o\left(\frac{\Delta P R_o}{2\text{mL}}\right)^s \int_\xi^1 \left(r - \frac{\lambda^2}{r}\right)^s dr if \lambda \le \xi \le 1 \end{cases} \tag{4}$$

λ is dimensionless since it was originally defined by Hanks and Larsen [28] as the ratio between the zero shear rate (maximum velocity) position λR and the outer radius R. Pressure drops can thus be directly evaluated by rearranging Equation (3). The thermal problem is instead solved by handling Equation (1c). In Newtonian fluids, where the dimensionless temperature $\theta = \frac{(T-T_e)}{q_w D_h/\lambda}$ (T_e: entrance temperature), the difference between the dimensionless bulk and wall temperatures in the fully developed region is analytically expressed as follows [29]:

$$\theta_b - \theta_w = \frac{\omega}{1+\omega}\frac{1}{M^2(1-\omega)^2}\left\{-\left[\frac{73}{48} - \frac{31}{18}B + \frac{11}{16}B^2 - \frac{1}{2B}\right] - \left[\frac{25}{48} - \frac{2}{9}B - \frac{5}{16}B^2\right]\omega^2 - \left[\frac{19}{36}B - \frac{11}{48}\right]\omega^4 + \frac{11}{48}\omega^6\right\} \quad (5)$$

where $M = 1 + \omega^2 - B$ and $B = \left(\omega^2 - 1\right)/\ln(\omega)$. The Nusselt number reads as $Nu = 1/(\theta_b - \theta_w)$. Such a formulation originates from the direct integration of the energy equation by considering the axial coordinate tending to infinity (fully developed region), and further mathematical manipulation based on energy considerations on the imposed boundary conditions. For further details on the analytical derivation, the reader is referred to the technical note by Lundberg et al. [30]. When non-Newtonian fluids are considered instead, the velocity profile of Equation (4) must be introduced in Equation (1c) and solved by separating variables and integrating twice. The solution steps were performed by means of the symbolic tool of Matlab© (v. R2019b); for the used flow behavior indexes n = 0.46 and n = 0.28, the Nusselt number results were equal to 6.107 and 6.170, respectively. It has to be underlined that annular sections present asymptotically better thermal performances than circular ones, and, for fixed fluid properties, the Nusselt number is only a function of the radius ratio, which thus represents the key parameter for engineering design [24].

2.4. Numerical Approach

The governing equations for the staggered helical finned section were solved numerically through the Ansys© Fluent code (v. 2023 R1) based on the second-order accurate finite volume method. For the finned annulus, all assumptions and conditions of Section 2.2 held, except for the axis symmetry. Conjugate heat transfer was additionally considered at the fluid–fins interfaces, which resulted in the imposed relations $T_s = T_f$ and $k_s \frac{\partial T_s}{\partial \hat{n}} = k_f \frac{\partial T_f}{\partial \hat{n}}$, where the subscripts s and f refer to solid and fluid, respectively, and $\hat{n}$ is the unit normal vector.

Both the annular and finned geometries were meshed by polyhedral elements in Ansys© Design Modeler (v. 2023 R1). Fifteen inflation layers were applied at the inner and outer walls of the fluid domain and at the base of the solid fins, with a first-layer height of 3×10^{-4} m and a growth rate equal to 1.1. Such a wall refinement was, in fact, necessary to obtain good resolution at the near-wall region, i.e., where the velocity and temperature gradients were expected to be significantly high. In Figure 3, the studied DPHE module is shown, along with the adopted mesh; the grid used for the bare annulus computations is additionally shown as a reference. Due to the intrinsic deep laminar flow conditions investigated in the present work, the resolution of the continuity and momentum governing equations was directly performed without any transformation or closure model. A pressure-based solver was selected. The Semi-Implicit Method for Pressure-Linked Equations (SIMPLE) algorithm was used for pressure–velocity coupling. The power-law model for the non-Newtonian fluids was implemented through the shear-rate-dependent method, which provided default minimum and maximum viscosity limits. Periodic simulations were implemented by specifying the mass flow rate through the annular section, with the upstream temperature equal to 300 K and the first-attempt pressure gradient equal to 0 Pa/m. The relaxation factor for the pressure gradient convergence was set equal to 0.5, with the number of sub-iterations in the pressure correction steps of the SIMPLE algorithm equal to 5. Specifically, in the definition of the streamwise-periodic pressure formulated by the software, the local pressure gradient was decomposed into the gradient of the periodic component and the gradient of the linearly varying component (treated as a force acting on the fluid in the momentum equation), with the latter being iterated until the set mass flow rate was achieved in the computational model. Default under-relaxation factors were used to allow for stable solution convergence. The solution was initialized through standard initialization. The absolute convergence criterion for all the residuals was set equal to 1×10^{-8}.

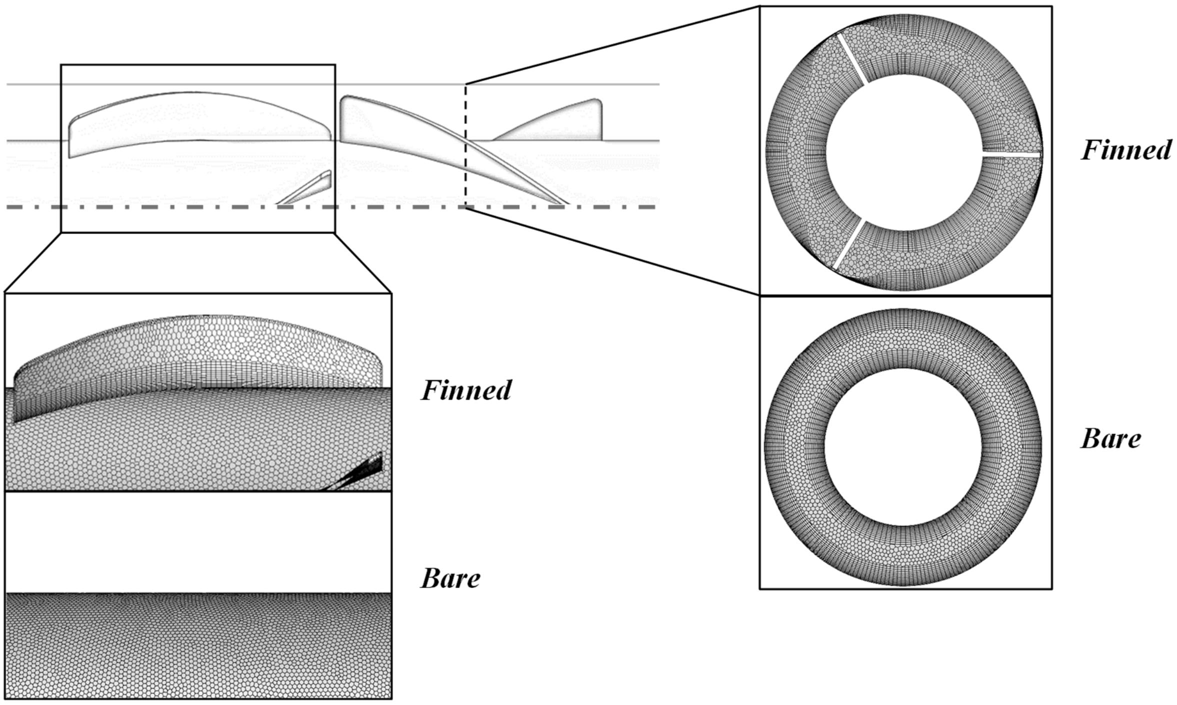

Figure 3. Details on the adopted meshing strategy for the finned and bare annuli.

3. Results

3.1. Grid Independence Analysis and Numerical Approach Validation

Grid independence analysis was performed for both the three-dimensional bare and finned annuli to ensure robust results of the numerical approach. The results that refer to only *Fluid 1* are reported in the present section. The sequentially refined meshes are listed in Table 1.

Table 1. Meshes adopted for grid independence analysis.

Bare Annulus		Finned Annulus	
Grid	**Number of Elements**	**Grid**	**Number of Elements**
A	281,483	A	522,437
B	552,797	B	1,796,547
C	1,224,531	C	4,391,979
D	2,303,367	D	8,919,136

The friction factor and the Nusselt number were chosen as meaningful quantities to check for grid independence. Specifically, the Fanning friction factor f and the Nusselt number Nu were defined as follows:

$$f = \Delta p_{x \to x+L}(D_o - D_i) / \left(2\rho W^2 L\right) \tag{6a}$$

$$Nu = \frac{h(D_o - D_i)}{k} \tag{6b}$$

where W is the average fluid velocity; ρ is the fluid density; and h is the convective heat transfer coefficient, defined as $h = q_w / \left(\overline{T}_w - \overline{T}_b\right)$, where $\overline{T}_w$ is the average wall temperature (evaluated at the surface A, i.e., the inner annulus wall) and $\overline{T}_b$ is the average bulk temperature, $\overline{T}_b = [T_b(x+L) - T_b(x)]/2$.

In Figure 4, f and Nu are plotted against the number of grid elements. For both geometries, the analyzed quantities stabilized after grid C (Table 1), underlining similar results for further refined meshes.

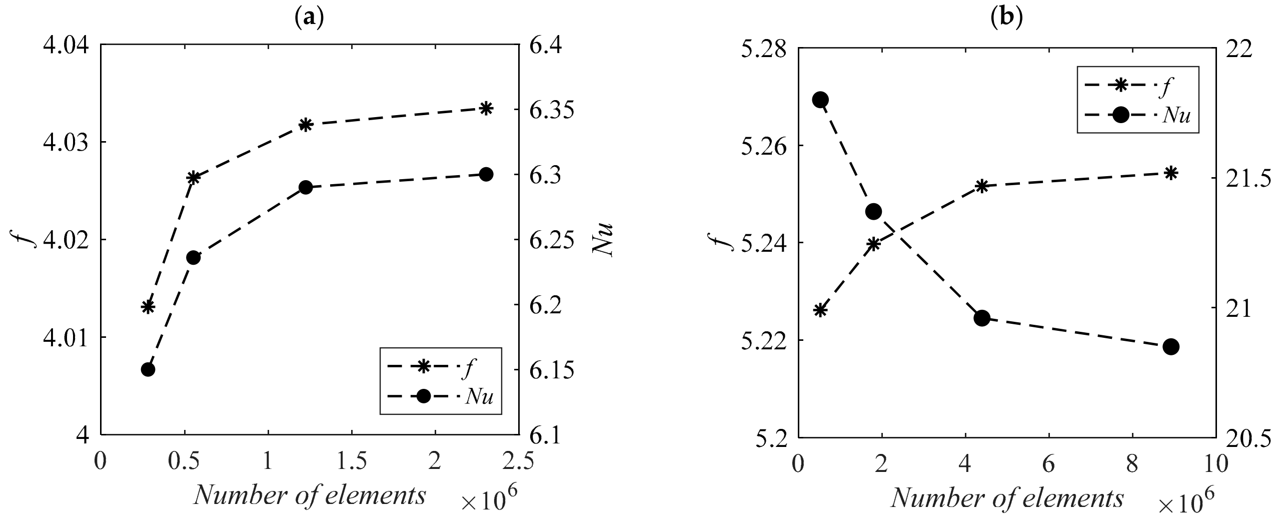

Figure 4. Grid independence analysis for the bare (**a**) and finned (**b**) annuli in terms of the friction factor and Nusselt number.

The grid independence analysis was additionally performed for the local features of the studied flow, such as the dimensionless velocity $u^* = \frac{u}{W}$ and the dimensionless temperature $\theta = \frac{(T - T_w)}{q_w D_h / k}$ profiles. In Figure 5, u^* and θ are plotted as functions of the dimensionless radial coordinate r/R_o along half of the annular passage for the four considered computational grids. Specifically, the reported profiles refer to the axial coordinate in between the two finned sections, i.e., at the fin interruption.

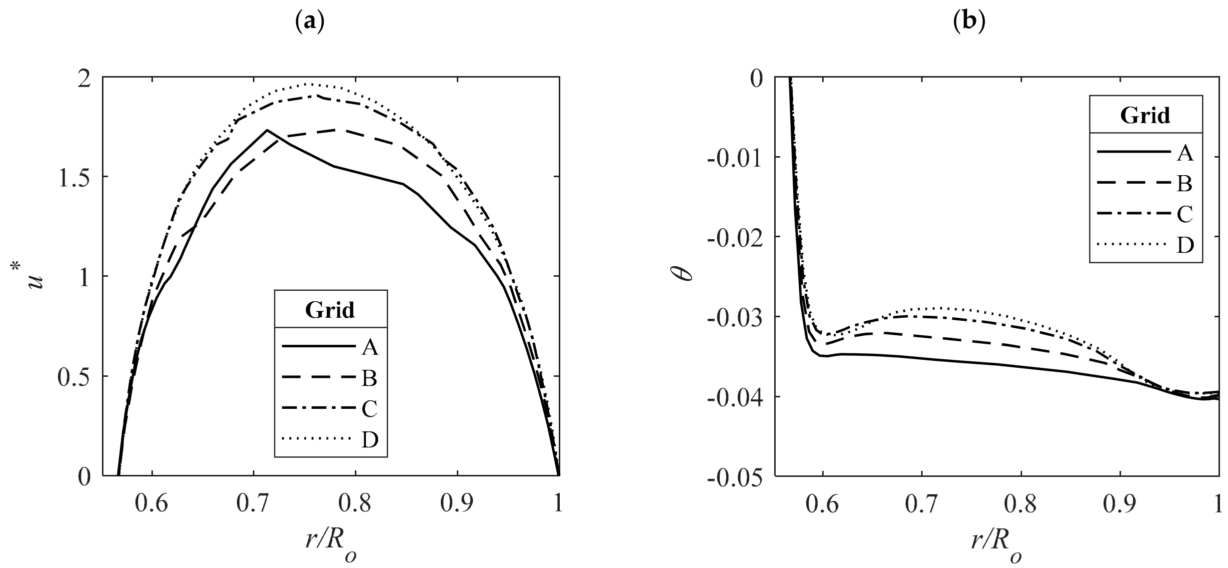

Figure 5. Grid independence analysis for the finned annulus in terms of the dimensionless velocity (**a**) and dimensionless temperature (**b**) profiles.

As is noticeable, for sequential increases in the number of mesh elements, the shown profiles tended to exhibit less spatial differences, in agreement with the stabilization of the global quantities of Figure 4 at higher number elements. Minor differences could be perceived between grids C and D in terms of u^* and θ. In other words, both the global and local thermofluidic characteristics of the investigated flow became independent of the grid elements above grid C. Hence, a good trade-off between the accuracy of the results and the computational time was achieved by means of grid C, and it was therefore used for the present validation and following numerical investigation.

To validate the numerical approach, the analytical results were compared with the ones from the bare annulus simulations. For the benchmark case, *Fluid 1* and Re_g = 4.9 were considered; for the sake of clarity, it has to be stressed that the generalized Reynolds number adopted in the present work reflected the one originally defined by Metzner and Reed [31]:

$$Re_g = \frac{\rho W^{2-n} D_h^n}{8^{n-1} m \left(\frac{3n+1}{4n}\right)^n} \tag{7}$$

where ρ is the fluid density and $D_h = D_o - D_i$ is the hydraulic diameter.

First, the friction factor and Nusselt number were compared to assess the goodness of the numerical results from a global standpoint. In Table 2, the analytical and numerical f and Nu are listed, along with their relative errors. Here, the discrepancy between the analytical and numerical solutions was rather limited, highlighting that the numerical approach successfully detected the main global features of the annular non-Newtonian flow.

Table 2. Comparison between the analytical and numerical friction factor and Nusselt number (*Fluid 1*, Re_g = 4.9).

	Analytical Solution	**Numerical Solution**	**Relative Error [%]**
f	4.031	4.032	0.2
Nu	6.107	6.290	3.0

Local thermofluidic features were instead analyzed by comparing the analytical and numerical solutions in terms of the dimensionless velocity and dimensionless temperature profile. Such a comparison is depicted in Figure 6, where the two quantities are plotted against the dimensionless radial coordinate.

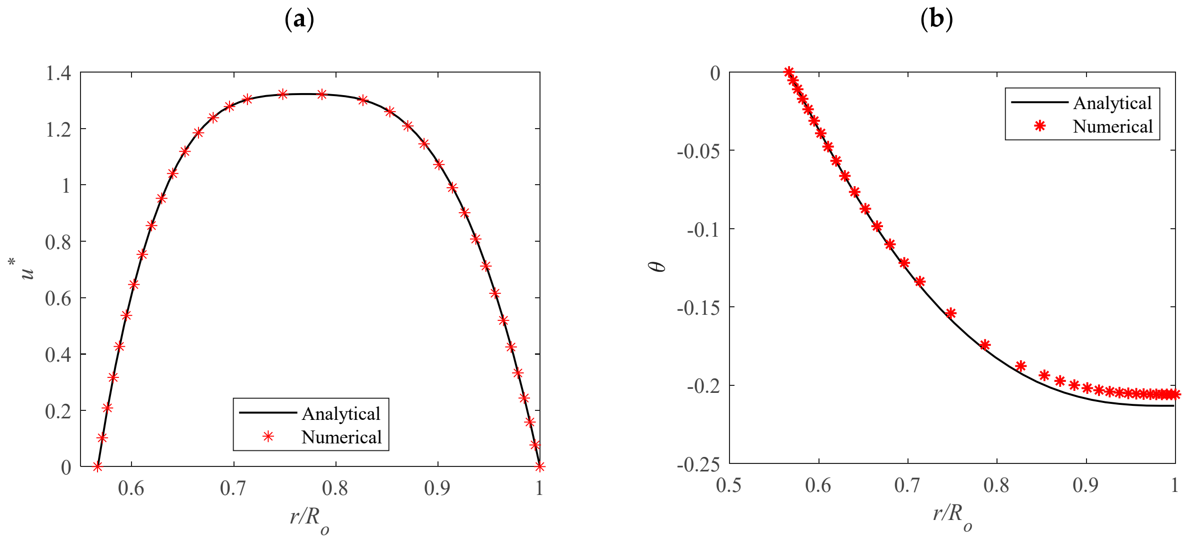

Figure 6. Analytical and numerical solutions. Dimensionless velocity (**a**); dimensionless temperature (**b**).

The numerical velocity profile of Figure 6a reflects with high accuracy the one analytically evaluated by Equation (4). For what concerns the dimensionless temperature profile (Figure 6b), the agreement between the numerical and analytical solutions was good, despite a slight deviation from the analytical data being perceivable at high r/R_o (i.e., close to the adiabatic outer wall), with a maximum absolute shift of about 3.4%. Such a discrepancy could have been due to numerical approximations introduced by the periodic convergence. To conclude, the provided global and local comparisons confirmed the robustness of the adopted numerical approach, as well as the consistency of the outputted results. Hence, the proposed numerical scheme was used for further investigations on the finned geometry.

3.2. Fluid Flow Characteristics

The effects of the newly proposed configuration on the fluid flow were first analyzed. The direction of the fluid flow across the finned module is outlined by the streamlines of Figure 7 for *Fluid 1*. Here, the presence of helical fins resulted in an induced swirl motion, which was expected to enhance the heat transfer performance according to previous literature works on swirling flow devices [16,17,32,33]. As soon as the twisted fins were interrupted, i.e., in the middle of the finned module, the streamlines drastically changed direction. Note that the fin interruption promoted fluid flow bifurcation, which could beneficially affect the overall boundary layer disruption and product thermalization. On one hand, the fluid followed longer paths, which resulted in increased residence time in the DPHE module with respect to the continuous helical fins. On the other hand, the same portion of fluid was forced to rearrange its radial position, which improved, at least to some extent, the overall mixing.

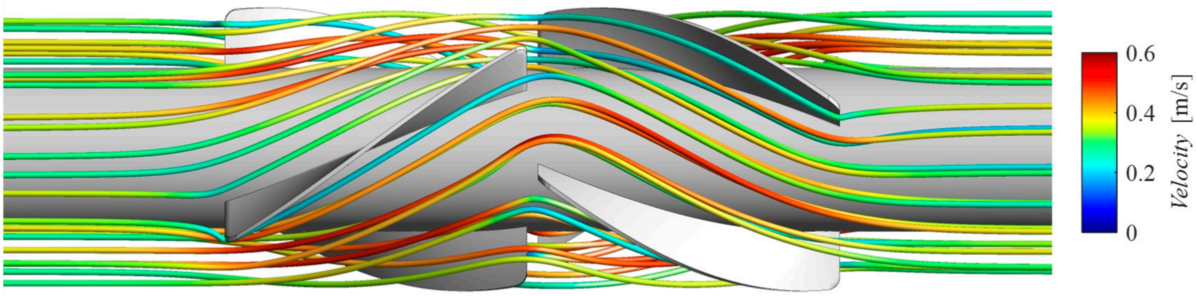

Figure 7. Streamlines at Re_g = 4.9.

The fluid flow behavior across the proposed DPHE module was further analyzed by considering five meaningful sections (Figure 8, fluid flowed from section 1 to section 5). The corresponding fluid velocity contours were evaluated and are shown in Figure 9 for Re_g = 4.9.

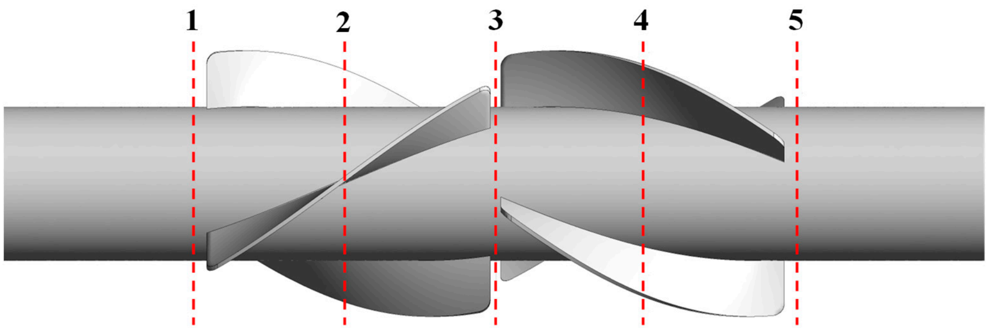

Figure 8. Reference for the fluid sections of interest (fluid flowing from section 1 to section 5).

In section 1, the fluid started accelerating close to one side of the fins due to an abrupt change in direction, while the opposite side exhibited flow deceleration and partial fluid stagnation. Such an unbalanced velocity distribution, which resulted from inertial effects induced by the fins, was expected to promote boundary layer disruption at the considered section [16]. In sections 2 and 4, the fluid was instead barely circumferentially accelerated, probably due to the deep laminar regime that characterized the studied flow [20]. In fact, the computed velocity contours were better approximated by those obtained through longitudinal fins [22,34], which confirmed the occurrence of dominant axial flows over the secondary ones. This could lead to poorer heat transfer augmentation guaranteed by the sole helical fins due to the low generalized Reynolds numbers considered in the present work (in agreement with [35]), underlining the importance of introducing additional flow disturbance by fin interruption. In section 3, the velocity contour highlighted the highest non-uniformity. As also observed in Figure 7, the fluid abruptly inverted its direction due to the presence of an interrupted staggered fins configuration. Moreover, the relative positioning of the fins resulted in an alternation of high- and low-velocity areas, which reflected the sudden reduction in the flow section within the fins and stagnation points at the fin edges. The velocity contours of sections 4 and 5 presented similar patterns to those of sections 2 and 1, respectively, although they locally varied due to obvious geometrical reasons. From the fields provided, it is interesting to note that the maximum velocity did not substantially vary along the module, which suggests limited pressure drops introduced by the fins.

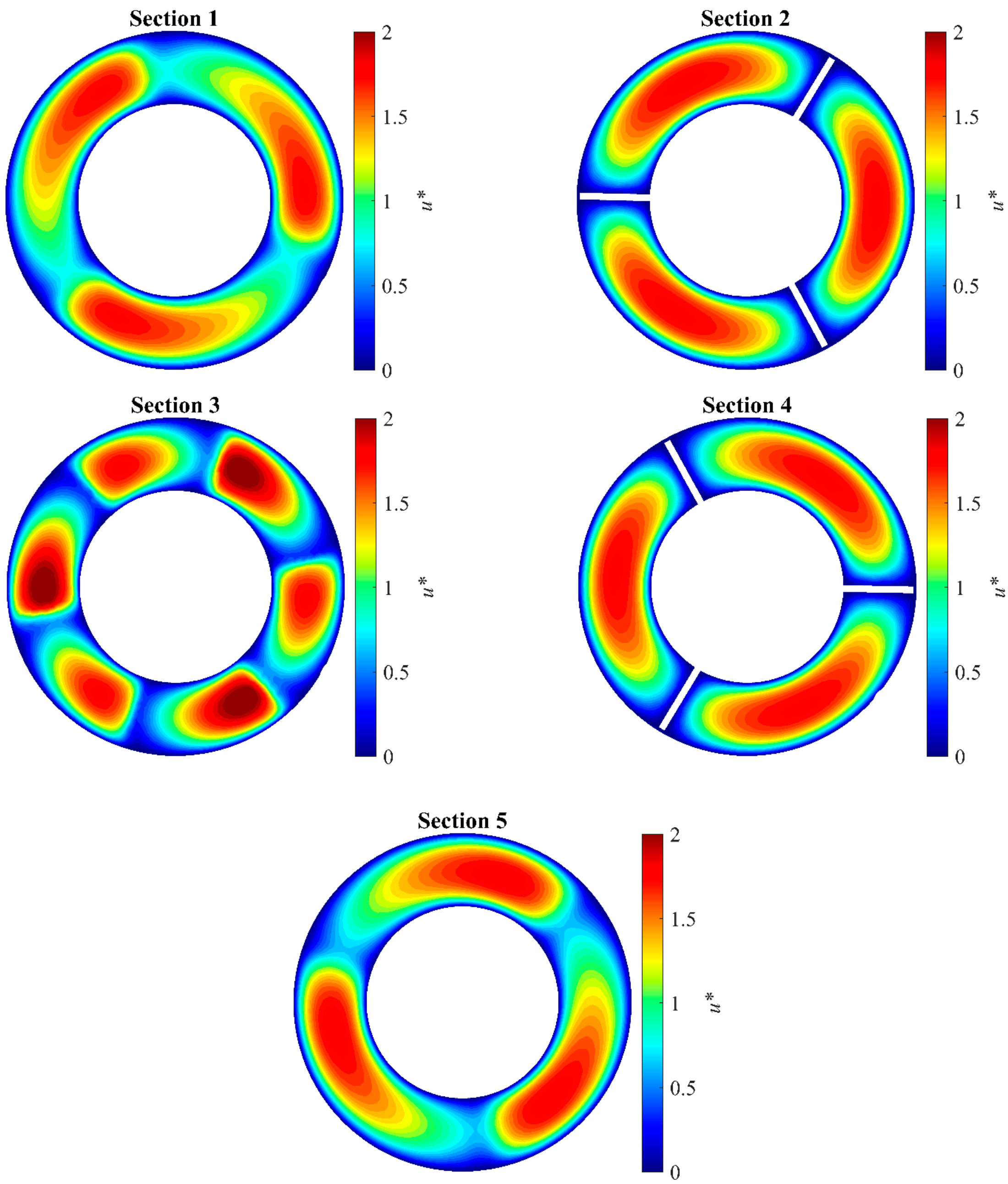

Figure 9. Dimensionless fluid velocity (sections of Figure 6).

3.3. Thermal Characteristics

After a local analysis of the dimensionless velocity fields, the local thermal effects that resulted from the proposed configuration were investigated in the same sections of interest (Figure 8). In Figure 10, the dimensionless temperature distributions that referred to $Re_g = 4.9$ are plotted. Specifically, the dimensionless temperature was computed by means of the definition of Section 3.1 by adopting the maximum fluid temperature at the wall. In section 1, θ presented, on average, large variations from the outer side to the inner, heated side of the annulus. In fact, for non-Newtonian fluids, the typically high Prandtl number yields thin thermal boundary layers that decrease thermal penetration [36], confirming the need for greater fluid thermalization through boundary layer disruption and efficient mixing. Nonetheless, the temperature distribution exhibited three main areas in which the heat better diffused into the fluid. By comparing the temperature contour with the velocity profile of Figure 9 (section 1), such diffusive areas were found to correspond to those having a maximum fluid velocity, i.e., best convective capabilities. The warmer areas tended to enlarge as soon as the fluid crossed the finned module from section 2 to section 5. In particular, section 5 had a more uniform dimensionless temperature distribution than that of section 1, which confirmed the advantages of the proposed solution in terms of the fluid thermalization due to the coupled effect of the boundary layer disruption and fluid mixing ensured by the analyzed geometry. This remark was additionally verified by the higher dimensionless temperature that resulted from the novel configuration with respect to that of the bare annulus (Figure 6b).

To further clarify the role of the finned module in the overall heat transfer process, the dimensionless temperature distribution of a representative fin of section 4 (Figure 10), θ_{fin}, is outlined in Figure 11. Specifically, θ_{fin} exhibited a rapid drop along the radial length from the base of the fin, and it then approached the fluid temperature. Note that the base of the fin had a negative dimensionless temperature; in fact, for the present study case, the heat transfer to the fluid performed even worse than pure conduction through the solid domain (stainless steel), which led to generally colder fin bases than the fluid in contact with the heated surface.

It could thus be concluded that heat was weakly exchanged between the fins and the fluid due to the low temperature differences. Such a remark was confirmed by the fact that the contours of Figure 8 did not exhibit any significant fluid temperature variations close to the fins, which suggested that thermofluidic interactions at the extended surfaces played an almost negligible role in the convective wall-to-fluid heat transfer. Such poor fins performance could be attributed to a combination of two different features of the considered problem: on one hand, the low thermal conductivity of the stainless steel reduced the amount of heat transferred from the base to the tip of the fins. It has to be pointed out that the material choice carried out in the present work was driven by technological reasons. In fact, stainless steel is widely employed in industrial processes (e.g., in the pharmaceutical, food and petroleum industries [37]), mainly due to its high corrosion resistance. Hence, other materials with better thermal properties, i.e., those that could enhance the heat transfer from the inner wall to the fluid through the fins, were intentionally discarded from the present analysis. On the other hand, the high Prandtl number that characterized the investigated flow greatly penalized the heat diffusion in the fluid at both the inner wall-to-fluid and the fin-to-fluid interfaces. The boundary layer disruption was hence confirmed to be the main heat transfer augmentation mechanism that took place in the studied staggered helical fins module, in agreement with what was observed in previous analyses [38].

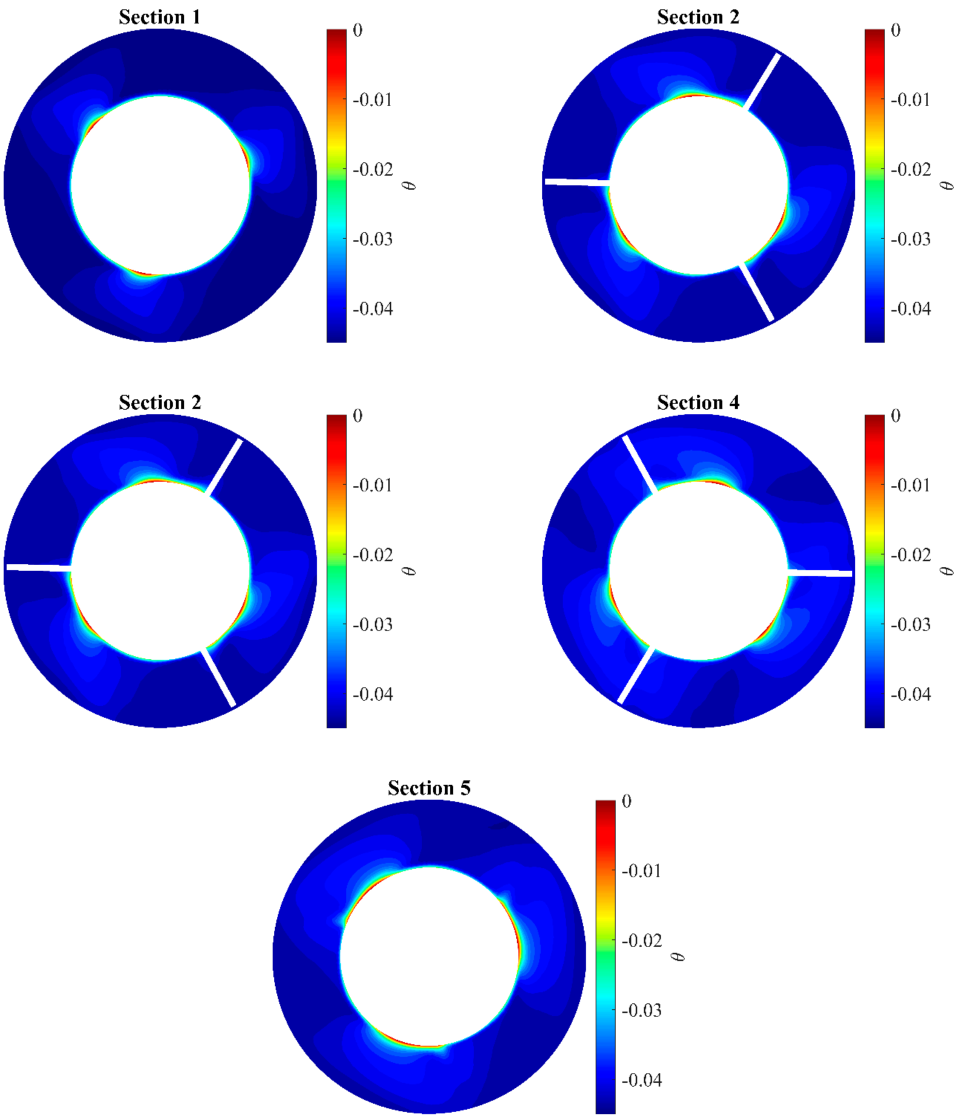

Figure 10. Fluid dimensionless temperature distributions (sections of Figure 6).

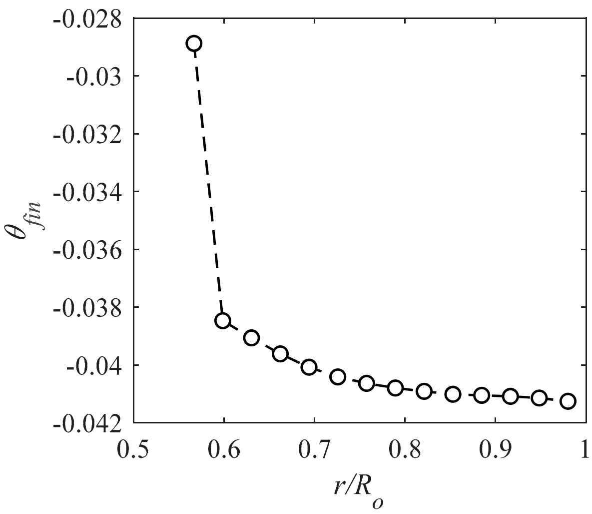

Figure 11. Dimensionless temperature distribution along a representative fin (section 4 of Figure 7).

3.4. Performance Augmentation of the Finned Heat Exchanger Module

The performance augmentation achieved through the novel finned DPHE module was finally assessed by reporting the main dimensionless quantities that defined the inner thermo-fluid dynamics, such as the friction factor and the Nusselt number, for the two fluids of interest. As mentioned in Section 2, the finned DPHE module was studied at different values of the generalized Reynolds number. In Figure 12, the friction factor (Figure 12a) and Nusselt number (Figure 12b) in the $NuPr_g^{-1}$ form are shown (Pr_g: generalized Prandtl number). To underline the performance augmentation achieved through fins, the results referred to the bare annulus were analytically computed from the definitions of Section 2.2 and included in the presented graphs. Specifically, the used formulation for the generalized Prandtl number reflected the one adopted in [39]:

$$Pr_g = \frac{c_p m}{k}\left(\frac{W}{D_i}\right)^{n-1} \quad (8)$$

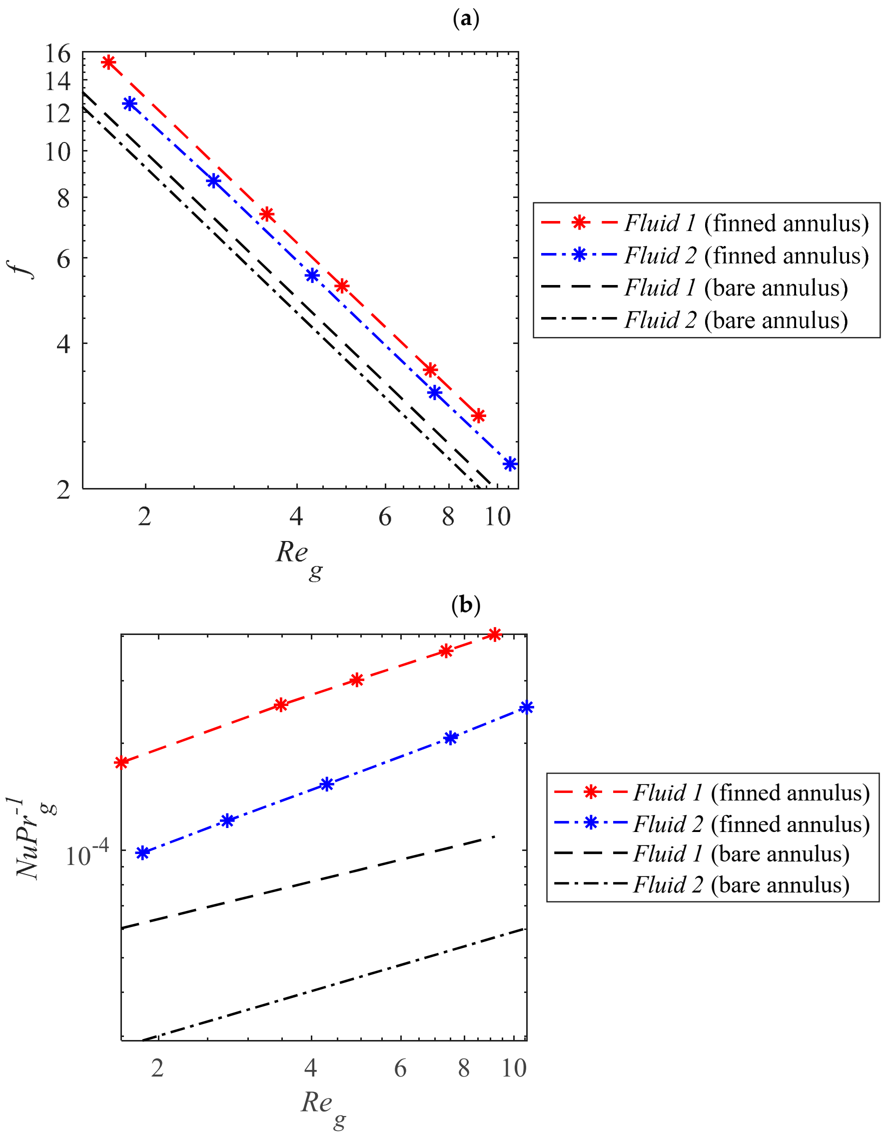

Figure 12. Friction factor (**a**) and Nusselt number in the $NuPr_g^{-1}$ form (**b**) for the finned and bare annuli. Analytical solution for the bare annulus; numerical solution for the finned annulus.

Note that the quantity $NuPr_g{}^{-1}$ was introduced here in place of the sole Nu since literature works usually relate the Nusselt number variations to those of the generalized Reynolds and Prandtl numbers [16,40].

In Figure 12a, a higher friction factor was observed for *Fluid 1*, i.e., a fluid having a higher flow behavior index, for both geometrical configurations, which confirmed what was expected from the available literature on non-Newtonian flows through annular sections. In fact, for the bare annulus under the laminar regime, the relationship between the generalized Reynolds number defined in [31] and the Fanning friction factor can be expressed, according to Ayas et al. [41], as

$$Re_g f = (2\psi - 16)n + 16 \tag{9}$$

ψ assumes different values depending on the considered cross-section and aspect ratios. Such a parameter was originally introduced by Delplace and Leuliet [42] to tackle the poor generalization in pressure drop predictions of power-law fluids for those cases in which the velocity profiles were characterized by higher complexity than simple cross-sections. It is interesting to note that when non-Newtonian, laminar flows through straight circular pipes are considered (ψ = 8), Equation (9) reduces to $f = 16/Re_g$. In other words, the friction factor completely drops its dependency on the flow behavior index.

For what concerns the heat transfer process, in Figure 12b, $NuPr_g{}^{-1}$ assumes higher values for the finned configuration. Similar to the friction factor trends, higher $NuPr_g{}^{-1}$ values were noticeable for *Fluid 1*, which respected the typical analogy between heat and momentum transfer [43]. Better thermal performances for the finned annulus configuration were thus accompanied by higher friction factors. When the finned and bare annuli were compared in terms of the investigated quantities, an increase in friction factor of about 30% led to an increase in $NuPr_g{}^{-1}$ of about 200%, which highlighted the great advantage of the proposed staggered fins solution in the augmentation of thermal performances over friction losses.

4. Discussion

A double-pipe heat exchanger with a novel staggered, interrupted fins configuration on the annulus side was numerically investigated to assess its heat transfer augmentation capability over the standard annular geometry. Such a configuration was specifically chosen since it was believed to enhance the boundary layer disruption mechanisms without extremely perturbing the fluid flow. Periodic simulations were performed for two power-law, non-Newtonian fluids under a deep laminar flow regime (generalized Reynolds number ranging from about 1.5 up to 11), and the numerical approach was successfully validated against analytical results for the bare annulus. The thermo-fluid dynamics that resulted from the novel geometry was investigated in terms of the dimensionless velocity and temperature contours along the finned module. The numerically evaluated friction factors and Nusselt numbers were finally compared with the ones of the reference geometry to assess the overall performance augmentation provided by the present geometry.

From the present study, the following main outcomes could be drawn:

- While the high pitch of the helical fins induced limited radial accelerations, the layout interruption resulted in higher velocity non-uniformity, which allowed for improved boundary layer disruption. Such a remark was confirmed by the better fluid thermalization achieved after the layout interruption.
- The heat exchanged at the extended surfaces played a negligible role in the overall convective heat transfer; for deep laminar flows that involved non-Newtonian, high-Prandtl fluids, the finned solutions solely behaved as stationary passive disruptors.
- The finned geometry highlighted an increase in the friction factor of about 30% with respect to the bare annulus. On the other hand, the Nusselt number, in the $NuPr_g{}^{-1}$ form, exhibited a more significant rise of about 200% with respect to the reference geometry.

To conclude, for the analyzed test conditions, the staggered fins performed better than the bare annulus, suggesting improved overall performances of the heat exchanger module. The provided results can thus be adopted to design promising passive solutions for heat transfer enhancement in deep laminar non-Newtonian flows through annular pipes. Further modifications in the proposed layout will be carried out in future developments to achieve morphological optimization of heat transfer performances.

Author Contributions: Conceptualization, S.R.; methodology, L.P.; software, L.P. and R.F.; validation, L.P.; formal analysis, S.R.; investigation, L.P.; resources, R.F.; data curation, L.P. and R.F.; writing—original draft preparation, L.P.; writing—review and editing, F.B. and R.F.; visualization, F.B.; supervision, F.B.; project administration, F.B. and S.R.; funding acquisition, S.R. All authors have read and agreed to the published version of the manuscript.

Funding: The authors would like to acknowledge financial support from PNRR-M4C2-I1.1—MUR Call for proposals n.104 of 02-02-2022—PRIN 2022—ERC sector PE8—Project title: MOOD4HEX—MOrphology Optimized Design for Heat EXchangers—Project Code 2022SJP2A5—CUP Code D53D23004040006—Funded by the European Union—NextGenerationEU. The authors would also like to acknowledge financial support from the PNRR MUR project ECS_00000033_ECOSISTER and from the CFT Group, Parma, Italy (https://www.cft-group.com/it/, accessed on 4 November 2024).

Data Availability Statement: The data presented in this study are available upon request from the corresponding author. The data are not publicly available due to the large dataset.

Conflicts of Interest: The authors declare no conflict of interest. The funders had no role in the design of this study; in the collection, analyses, or interpretation of the data; in the writing of this manuscript; or in the decision to publish the results.

Nomenclature

Symbol	Quantity	SI Unit
$\hat{n}$	Unit normal vector	-
A	Heat transfer area	m^2
c_p	Specific heat	J/kgK
D	Diameter	m
f	Fanning friction factor	-
k	Thermal conductivity	W/mK
L	Length	m
m	Consistency index	Pa s^n
n	Flow behavior index	-
Nu	Nusselt number	-
p	Pressure	Pa
Pr	Prandtl number	-
q	Heat flux	W/m^2
Q_m	Mass flow rate	kg/s
Q_v	Volumetric flow rate	m^3/s
R	Radius	m
r	Radial coordinate	-
Re	Reynolds number	-
u	Velocity vector	m/s
u^*	Dimensionless velocity	-
W	Average velocity	m/s
x	Axial coordinate	-
η	Apparent viscosity	Pa s
α	Thermal diffusivity	m^2/s
θ	Dimensionless temperature	-
λ	Radial location of maximum velocity	-
ρ	Density	kg/m^3
ψ	Geometrical parameter	-
ω	Radius ratio	-

τ	Stress tensor	Pa
Subscripts, superscripts		
g	Generalized	
b	Bulk	
e	Entrance	
h	Hydraulic	
o	Outer	
i	Inner	
w	Wall	
s	Solid	
f	Fluid	
fin	Finned domain (solid)	

References

1. Dincer, I. Renewable energy and sustainable development: A crucial review. *Renew. Sustain. Energy Rev.* **2000**, *4*, 157–175. [CrossRef]
2. Li, H.; Wang, Y.; Han, Y.; Li, W.; Yang, L.; Guo, J.; Liu, Y.; Zhang, J.; Zhang, M.; Jiang, F. A comprehensive review of heat transfer enhancement and flow characteristics in the concentric pipe heat exchanger. *Powder Technol.* **2022**, *397*, 117037. [CrossRef]
3. Bhattacharyya, S.; Vishwakarma, D.K.; Srinivasan, A.; Soni, M.K.; Goel, V.; Sharifpur, M.; Ahmadi, M.H.; Issakhov, A.; Meyer, J. Thermal performance enhancement in heat exchangers using active and passive techniques: A detailed review. *J. Therm. Anal. Calorim.* **2022**, *147*, 9229–9281. [CrossRef]
4. Tavousi, E.; Perera, N.; Flynn, D.; Hasan, R. Heat transfer and fluid flow characteristics of the passive method in double tube heat exchangers: A critical review. *Int. J. Thermofluids* **2023**, *17*, 100282. [CrossRef]
5. Marzouk, S.A.; Al-Sood, M.M.A.; El-Said, E.M.S.; Younes, M.M.; El-Fakharany, M.K. A comprehensive review of methods of heat transfer enhancement in shell and tube heat exchangers. *J. Therm. Anal. Calorim.* **2023**, *148*, 7539–7578. [CrossRef]
6. Ghanbari, S.; Javaherdeh, K. Thermal performance enhancement in perforated baffled annuli by nanoporous graphene non-Newtonian nanofluid. *Appl. Therm. Eng.* **2020**, *167*, 114719. [CrossRef]
7. Vishkaei, M.Y.; Javaherdeh, K. Evaluating the efficiency and effectiveness of non-Newtonian fluid flow in a double-pipe heat exchanger with porous medium via numerical simulation. *Numer. Heat Transf. Part A Appl.* **2024**, 1–22. [CrossRef]
8. Vishkaei, M.Y.; Javaherdeh, K. Experimental investigation of the effects of metal foam porous rings on non-Newtonian fluid flow in a double pipe heat exchanger. *Int. Commun. Heat Mass Transf.* **2024**, *158*, 107950. [CrossRef]
9. Poursharif, Z.; Salarian, H.; Javaherdeh, K.; Nimvari, M.E. Numerical simulation of heat transfer on nanofluid flow in an annular pipe with simultaneous embedding of porous discs and triangular fins. *J. Chin. Inst. Eng.* **2021**, *44*, 158–169. [CrossRef]
10. Wang, Y.; Oon, C.S.; Foo, J.-J.; Tran, M.-V.; Nair, S.R.; Low, F.W. Numerical investigation of thermo-hydraulic performance utilizing clove-treated graphene nanoplatelets nanofluid in an annular passage with perforated curve fins. *Results Eng.* **2022**, *17*, 100848. [CrossRef]
11. Hadidi, H.; Mousavi, S.M.; Ghalambaz, M. Numerical study of MHD natural heat transfer of non-Newtonian, carbon nanotube-water nanofluid inside an internally finned annulus. *Eur. Phys. J. Plus* **2021**, *136*, 960. [CrossRef]
12. Mozafarie, S.S.; Javaherdeh, K.; Ghanbari, O. Numerical simulation of nanofluid turbulent flow in a double-pipe heat exchanger equipped with circular fins. *J. Therm. Anal. Calorim.* **2020**, *143*, 4299–4311. [CrossRef]
13. Gnanavel, C.; Saravanan, R.; Chandrasekaran, M. Heat transfer augmentation by nano-fluids and circular fin insert in double tube heat exchanger—A numerical exploration. *Mater. Today Proc.* **2020**, *21*, 934–939. [CrossRef]
14. Vaisi, A.; Moosavi, R.; Lashkari, M.; Soltani, M.M. Experimental investigation of perforated twisted tapes turbulator on thermal performance in double pipe heat exchangers. *Chem. Eng. Process.—Process. Intensif.* **2020**, *154*, 108028. [CrossRef]
15. Awais, M.; Bhuiyan, A.A. Recent advancements in impedance of fouling resistance and particulate depositions in heat exchangers. *Int. J. Heat Mass Transf.* **2019**, *141*, 580–603. [CrossRef]
16. Mozafarie, S.S.; Javaherdeh, K. Numerical design and heat transfer analysis of a non-Newtonian fluid flow for annulus with helical fins. *Eng. Sci. Technol. Int. J.* **2019**, *22*, 1107–1115. [CrossRef]
17. Karimi, A.; Al-Rashed, A.A.; Afrand, M.; Mahian, O.; Wongwises, S.; Shahsavar, A. The effects of tape insert material on the flow and heat transfer in a nanofluid-based double tube heat exchanger: Two-phase mixture model. *Int. J. Mech. Sci.* **2019**, *156*, 397–409. [CrossRef]
18. El Maakoul, A.E.; Laknizi, A.; Saadeddine, S.; Abdellah, A.B.; Meziane, M.; Metoui, M.E. Numerical design and investigation of heat transfer enhancement and performance for an annulus with continuous helical baffles in a double-pipe heat exchanger. *Energy Convers. Manag.* **2017**, *133*, 76–86. [CrossRef]
19. Shah, R.K.; London, A.L. *Laminar Flow Forced Convection in Ducts: A Source Book for Compact Heat Exchanger Analytical Data*; Academic Press: Cambridge, MA, USA, 2014.
20. Yu, D.; Jeon, W.; Kim, S.J. Analytic study on pressure drop and heat transfer characteristics for low reynolds number flow in spirally finned tubes. *Int. J. Heat Mass Transf.* **2020**, *158*, 119849. [CrossRef]

21. Mohsen, O.A.; Muhammed, M.A.R.; Hasan, B.O. Heat Transfer Enhancement in a Double Pipe Heat Exchanger Using Different Fin Geometries in Turbulent Flow. *Iran. J. Sci. Technol. Trans. Mech. Eng.* **2021**, *45*, 461–471. [CrossRef]
22. El Maakoul, A.; Feddi, K.; Saadeddine, S.; Ben Abdellah, A.; El Metoui, M. Performance enhancement of finned annulus using surface interruptions in double-pipe heat exchangers. *Energy Convers. Manag.* **2020**, *210*, 112710. [CrossRef]
23. Wang, L.; Lei, Y.; Jing, S. Performance of a Double-Tube Heat Exchanger with Staggered Helical Fins. *Chem. Eng. Technol.* **2022**, *45*, 953–961. [CrossRef]
24. Bergman, T.L.; Lavine, A.S.; Incropera, F.P.; Dewitt, D.P. *Fundamentals of Heat and Mass Transfer*; John Wiley & Sons: Hoboken, NJ, USA, 2011.
25. Schlichting, H.; Gersten, K. *Boundary-Layer Theory*; Springer: Berlin/Heidelberg, Germany, 2016.
26. Barbana, C.; El-Omri, A. Viscometric Behavior of Reconstituted Tomato Concentrate. *Food Bioprocess Technol.* **2009**, *5*, 209–215. [CrossRef]
27. Kubo, M.T.K.; Baicu, A.; Erdogdu, F.; Poças, M.F.; Silva, C.L.M.; Simpson, R.; Vitali, A.A.; Augusto, P.E.D. Thermal processing of food: Challenges, innovations and opportunities. A position paper. *Food Rev. Int.* **2023**, *39*, 3344–3369. [CrossRef]
28. Hanks, R.W.; Larsen, K.M. The Flow of Power-Law Non-Newtonian Fluids in Concentric Annuli. *Ind. Eng. Chem. Fundam.* **1979**, *18*, 33–35. [CrossRef]
29. Reynolds, W.; Lundberg, R.; McCuen, P. Heat transfer in annular passages. General formulation of the problem for arbitrarily prescribed wall temperatures or heat fluxes. *Int. J. Heat Mass Transf.* **1963**, *6*, 483–493. [CrossRef]
30. Lundberg, R.E.; Reynolds, W.C.; Kays, W.M. *Heat Transfer with Laminar Flow in Concentric Annuli with Constant and Variable Wall Temperature with Heat Flux*; National Aeronautics and Space Administration: Washington, DC, USA, 1963.
31. Metzner, A.B.; Reed, J.C. Flow of non-newtonian fluids—Correlation of the laminar, transition, and turbulent-flow regions. *AIChE J.* **1955**, *1*, 434–440. [CrossRef]
32. Shahsavar, A.; Bakhshizadeh, M.A.; Arici, M.; Afrand, M.; Rostami, S. Numerical study of the possibility of improving the hydrothermal performance of an elliptical double-pipe heat exchanger through the simultaneous use of twisted tubes and non-Newtonian nanofluid. *J. Therm. Anal. Calorim.* **2021**, *143*, 2825–2840. [CrossRef]
33. Taheran, E.; Javaherdeh, K. Experimental investigation on the effect of inlet swirl generator on heat transfer and pressure drop of non-Newtonian nanofluid. *Appl. Therm. Eng.* **2019**, *147*, 551–561. [CrossRef]
34. Wang, Q.-W.; Lin, M.; Zeng, M.; Tian, L. Computational analysis of heat transfer and pressure drop performance for internally finned tubes with three different longitudinal wavy fins. *Heat Mass Transf.* **2008**, *45*, 147–156. [CrossRef]
35. Karimi, J.R.C.G. Review and Assessment of Pulsating Heat Pipe Mechanism for High Heat Flus Electronic Cooling. In Proceedings of the Ninth Intersociety Conference on Thermal and Thermomechanical Phenomena in Electronic Systems, Las Vegas, NV, USA, 1–4 June 2004; pp. 1–18.
36. Metzner, A.B.; Friend, P.S. Heat Transfer to Turbulent Non-Newtonian Fluids. *Ind. Eng. Chem.* **1959**, *51*, 879–882. [CrossRef]
37. Zaffora, A.; Di Franco, F.; Santamaria, M. Corrosion of stainless steel in food and pharmaceutical industry. *Curr. Opin. Electrochem.* **2021**, *29*, 100760. [CrossRef]
38. Mousa, M.H.; Miljkovic, N.; Nawaz, K. Review of heat transfer enhancement techniques for single phase flows. *Renew. Sustain. Energy Rev.* **2021**, *137*, 110566. [CrossRef]
39. Farajzadeh, M.; Tohidi, A. Mixing and heat transfer enhancement of power-law fluids inside helically coiled tube by chaotic advection. *J. Non-Newtonian Fluid Mech.* **2019**, *274*, 104202. [CrossRef]
40. Rennie, T.J.; Raghavan, G.V. Thermally dependent viscosity and non-Newtonian flow in a double-pipe helical heat exchanger. *Appl. Therm. Eng.* **2007**, *27*, 862–868. [CrossRef]
41. Ayas, M.; Skocilas, J.; Jirout, T. Friction factor of shear thinning fluids in non-circular ducts—A simplified approach for rapid engineering calculation. *Chem. Eng. Commun.* **2021**, *208*, 1209–1217. [CrossRef]
42. Delplace, F.; Leuliet, J. Generalized Reynolds number for the flow of power law fluids in cylindrical ducts of arbitrary cross-section. *Chem. Eng. J. Biochem. Eng. J.* **1995**, *56*, 33–37. [CrossRef]
43. Mahulikar, S.P.; Herwig, H. Fluid friction in incompressible laminar convection: Reynolds' analogy revisited for variable fluid properties. *Eur. Phys. J. B* **2008**, *62*, 77–86. [CrossRef]